Available online at www.sciencedirect.com
ScienceDirect
International Journal of Solids and Structures 45 (2008) 3769–3778
INTERNATIONAL JOURNAL OF SOLIDS AND STRUCTURES
www.elsevier.com/locate/ijsolstr

Neck development in metal/elastomer bilayers under dynamic stretchings

Zhenyu Xue [a,*], John W. Hutchinson [b]

[a] Department of Engineering Mechanics, Tsinghua University, Beijing 100084, China
[b] School of Engineering and Applied Sciences, Harvard University, Cambridge, MA 02138, USA

Received 13 June 2007; received in revised form 5 October 2007
Available online 22 October 2007

Abstract

Dynamic stretching of bilayer plates comprised of an elastomer layer bonded to a metal layer is studied with emphasis on neck development under plane strain. Neck retardation and multiple necks in the metal layer are promoted by the elastomer layer under quasi-static conditions and also by inertia in the all-metal layer under dynamic stretching. The present study explores the interaction of these two effects under the assumption that ductility is unlimited. The study reveals the roles of the elastomer modulus, the metal strength and the rate of stretching in giving rise to necking retardation.

Keywords: Necking; Bilayer; Dynamic stretching; Plasticity

1. Introduction

The onset of a necking instability during stretching of metal rods and sheets is usually the first step in the failure process with localization of strain giving rise to microscopic damage within the neck which progresses to failure. In many polymers, necking is closely related to the drawing process wherein initial strain localization saturates without damage such that the neck then spreads along the entire length of the rod or sheet. The stress–strain behavior of many elastomers is such that necking instabilities do not occur at all. Bilayers composed of well bonded combinations of metal and elastomer (or polymer) layers can be more resistant to necking than a single metal sheet in the sense that the strain at which necking starts can be larger. The onset of necking under quasi-static tension occurs when the average true stress becomes equal to the overall tangent modulus, as originally elucidated by Considere over 100 years ago. For the bilayer, as discussed by Xue and Hutchinson (2007), the reduction in the tangent modulus of the metal with increasing strain is counteracted by the undiminished tangent modulus of the elastomer such that the bilayer attains the Considere condition at larger strains. The delay in necking can even promote more energy absorption prior to necking in a bilayer relative to that in an all-metal sheet of the same mass/per area if the relative properties of the two

* Corresponding author. Tel.: +86 10 62781465; fax: +86 10 62771113.
E-mail address: xuezy@mail.tsinghua.edu.cn (Z. Xue).

0020-7683/$ - see front matter © 2007 Elsevier Ltd. All rights reserved.
doi:10.1016/j.ijsolstr.2007.10.006

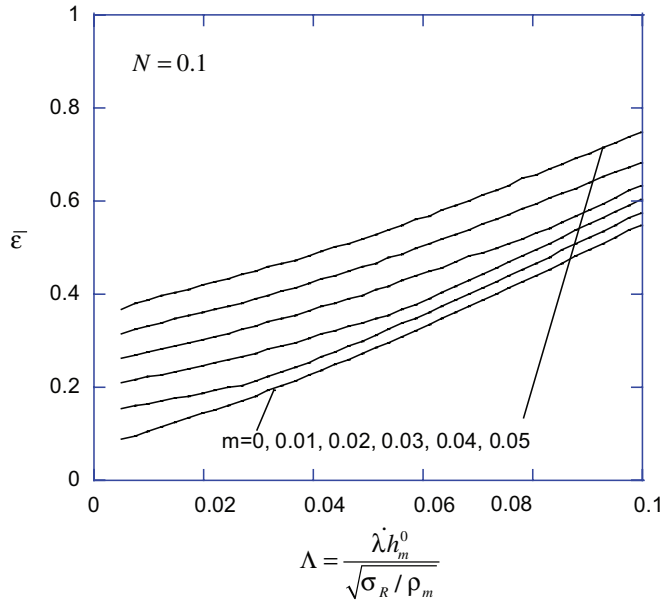

Fig. 1. Trends in the overall strain at necking as dependent on the dimensionless stretch-rate and the exponent characterizing the material rate-dependence for an all-metal plate subject to plane strain tension. The power-law relation, $\sigma/\sigma_Y = (\varepsilon/\varepsilon_Y)^N(\dot{\varepsilon}/\dot{\varepsilon}_R)^m$, governs material behavior in uniaxial tension. The trends assume small initial geometric imperfections as described by Xue et al. (in press). There is no dependence on σ_Y or ε_Y, and the dependence on the reference strain-rate, $\dot{\varepsilon}_R$, is very weak.

constituents are favorable. Specifically, for a combination of a Hookean elastomer bonded to steel characterized by power-law hardening having density ratio, $\rho_e/\rho_m = 0.14$, the condition for enhanced energy absorption per mass of bilayer is $h_e^0 E_e/(h_m^0 \sigma_R) > 0.1$, where h_e^0/h_m^0 is the elastomer/metal sheet thickness ratio, E_e is the ground state Young's modulus of the elastomer, and σ_R is the metal flow stress in uniaxial tension at a strain of unity (Xue and Hutchinson, 2007).

Material rate-dependence can also significantly retard the onset of necking in stretching (Woodford, 1969; Hutchinson and Neale, 1977), as can inertia when the rate of stretching is high (Shenoy and Freund, 1999). Fig. 1 from Xue et al. (in press) illustrates the effect of stretching rate, $\dot{\lambda}$, on the strain at the onset of necking in plane strain stretching for all-metal sheets with a power-law rate-dependence. These trends have been computed under the assumption that no microscopic material damage occurs. For power-law material rate sensitivity, significant neck retardation persists in the quasi-static, inertia-free limit at low stretch rates. The dimensionless parameter measuring the influence of inertial effects is $\Lambda \equiv \dot{\lambda} h_m^0/\sqrt{\sigma_R/\rho_m}$, where h_m^0 is the initial thickness of the sheet, ρ_m is the density of the metal, and σ_R is the reference stress introduced earlier. A distinctive feature of necking under dynamic stretching when $\Lambda > 0.01$ is the occurrence of multiple necks with separation between necks typically on the order of several times the sheet thickness. Multiple necks can also occur under quasi-static stretching of a bilayer when the elastomer layer is sufficiently stiff and thick (Li and Suo, 2006).

The present study explores the effects of dynamic stretching on metal/elastomer bilayers. As the introductory remarks above suggests, it will be of interest to focus on neck retardation and multiple neck formation. The study consists of a systematic analysis of a specific model carried out using the finite element method with the commercial software ABAQUS/Explicit. To isolate the combined effects of inertia and the elastomer layer, it will be assumed that the ductility of the two materials is not affected by microscopic damage.

2. Computational model of neck development of a bilayer under dynamic stretching

A bilayer plate comprised of a metal layer bonded to an elastomer layer under plane strain tensile straining at a constant stretching rate is considered as depicted in Fig. 2. The half-section of the symmetric bilayer plate

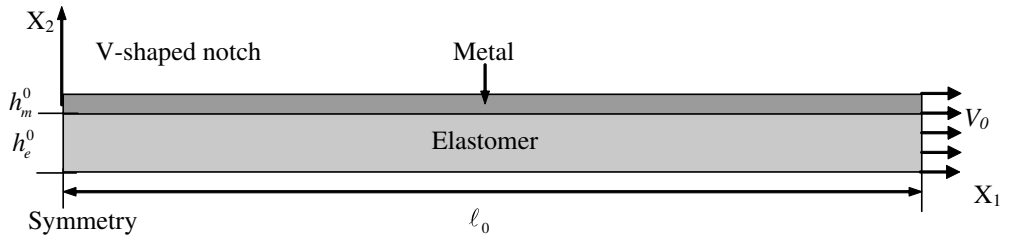

Fig. 2. Schematic diagram of a the right half of bilayer plate undergoing uniform overall plane strain stretching. A small V-shaped geometric is introduced at the center of the plate to trigger necking.

in the undeformed state has length l_0 with thickness h_{m}^0 for the metal layer and h_{e}^0 for the elastomer layer, respectively. The bilayer is constrained to undergo plane strain deformation. To investigate neck evolution, a V-shaped notch at the center of the full bilayer of $0.2h_{\mathrm{m}}^0$ half-width and $0.02h_{\mathrm{m}}^0$ depth is introduced at the top surface of the metal layer to trigger the onset of necking. Tractions on the top surface of metal layer and the bottom surface of elastomer layer are taken to be zero. The location of a material point in the undeformed state is denoted by Cartesian coordinates (X_1,X_2). The symmetry plane at the left end of the section at $X_1 = 0$ has zero horizontal displacement and zero shear traction. The right end at $X_1 = l_0$ is also subject to zero shear traction, and it is moved horizontally with constant velocity V_0 such that the length of the section at any time, t, is $l = l_0 + V_0 t$. With $\lambda = l/l_0$ as the overall stretch, the overall stretch-rate, $\dot{\lambda} = V_0/l_0$, is thereby prescribed to be constant. Reasonable initial conditions must be imposed in modeling behavior consistent with a long plate under a uniform stretch rate. A bilayer at rest subject to a suddenly imposed velocity on the right end can experience an intense plastic wave which immediately localizes as a neck before the wave even propagates from the right end (Needleman, 1991). An initial condition that models uniform stretching conditions is $V_1 = \dot{\lambda} X_1$ at $t = 0$ (Xue et al., in press).

For the metal, the elasticity is isotropic with Young's modulus E_{m}, Poisson's ratio ν_{m} and the density is ρ_{m}. Material rate-dependence is not considered. A power-law function is used to characterize the uniaxial tensile behavior such that the true stress-logarithmic strain relation is given by

$$\begin{cases} \sigma = E_{\mathrm{m}}\varepsilon, & \varepsilon \leqslant \sigma_{\mathrm{Y}}/E_{\mathrm{m}} \\ \sigma = \sigma_{\mathrm{R}}\varepsilon^N = \sigma_{\mathrm{Y}}\left(\frac{E_{\mathrm{m}}\varepsilon}{\sigma_{\mathrm{Y}}}\right)^N, & \varepsilon > \sigma_{\mathrm{Y}}/E_{\mathrm{m}} \end{cases} \tag{1}$$

where σ is the true stress, σ_{Y} is the initial yield stress, N is the strain hardening exponent, and the reference stress defined earlier is $\sigma_{\mathrm{R}} = \sigma_{\mathrm{Y}}^{1-N} E_{\mathrm{m}}^N$. The standard Mises flow law is assumed: $\dot{\varepsilon}_{ij}^P = 3\dot{\varepsilon}^p s_{ij}/2\sigma_{\mathrm{e}}$ where s_{ij} is the stress deviator, $\sigma_{\mathrm{e}} = \sqrt{3 s_{ij} s_{ij}/2}$ and $\dot{\varepsilon}_{\mathrm{e}}^P = \sqrt{2\dot{\varepsilon}_{ij}^P \dot{\varepsilon}_{ij}^P/3}$.

The elastomer is modeled as a near-incompressible Mooney–Rivlin material with density ρ_{e}. Such a material model is provided in ABAQUS/Explicit where the strain energy potential of the elastomer is specified in terms of three coefficients: C_{10}, C_{01}, and D. The multi-axial stress–strain behavior is thereby fully determined. The initial shear modulus μ_{e}, Poisson's ratio ν_{e}, ground state Young's modulus E_{e}, and bulk modulus K_{e} are related to C_{10}, C_{01}, and D via

$$\mu_{\mathrm{e}} = 2(C_{10} + C_{01}), \quad E_{\mathrm{e}} = 2(1 + \nu_{\mathrm{e}})\mu_{\mathrm{e}} \text{ and } K_{\mathrm{e}} = 2/D. \tag{2}$$

For the specific choices made for the three coefficients (see Table 1), the elastomer is similar to a Neo-Hookean material. We will take the ground state modulus, E_{e}, as the parameter defining the material stiffness in the discussion in the sequel.

Even when the geometry of the initial imperfection is fixed and the metal strain hardening index, N, and ν_{m} are prescribed, the set of dimensionless parameters governing the problem is large:

$$\Lambda = \frac{\dot{\lambda} h_{\mathrm{m}}^0}{\sqrt{\sigma_{\mathrm{R}}/\rho_{\mathrm{m}}}}, \ \frac{E_{\mathrm{e}}}{\sigma_{\mathrm{R}}}, \ \frac{h_{\mathrm{e}}^0}{h_{\mathrm{m}}^0}, \ \frac{\rho_{\mathrm{e}}}{\rho_{\mathrm{m}}}, \ \frac{\sigma_{\mathrm{R}}}{E_{\mathrm{m}}}, \ \frac{\ell_0}{h_{\mathrm{m}}^0} \tag{3}$$

Table 1
Material parameters used in the calculations

E_e/σ_R	E_e (MPa)	μ_e (MPa)	K_e (MPa)	C_{10} (MPa)	C_{01} (MPa)	D (1/MPa)
0.25	28.5	9.56	475	4.5980	0.18392	4.2105e−3
0.50	57	19.1	950	9.1959	0.36784	2.1053e−3
0.75	85.5	28.7	1425	13.794	0.55176	1.4035e−3
1.00	114	38.3	1900	18.392	0.73567	1.0526e−3
1.25	142.5	47.8	2375	22.990	0.91959	8.4211e−4

The bilayer half-length will be taken sufficiently long ($\ell_0/h_m^0 = 20$) such that results of interest are independent of ℓ_0/h_m^0. The parameter σ_R/E_m is unimportant because elasticity of the metal has little effect in the range of strains when necking occurs. However, the other dimensionless parameters all influence the phenomena discussed below. For this reason, the parameters space has been limited by restricting attention to a metal representative of an aluminum with both low hardening and low strength having $\rho_m = 2700\ \text{kg/m}^3$, $E_m = 70$ GPa, $\nu_m = 0.3$, $\sigma_Y = 100$ MPa, $N = 0.02$, and $\sigma_R = 114$ MPa. Moreover, the density of all the elastomers considered have fixed density $\rho_e = 1100\ \text{kg/m}^3$ such that for all cases considered, $\rho_e/\rho_m = 0.407$. The remaining dimensionless parameters are:

$$\Lambda = \frac{\dot{\lambda} h_m^0}{\sqrt{\sigma_R/\rho_m}},\ \frac{E_e}{\sigma_R},\ \frac{h_e^0}{h_m^0} \tag{4}$$

The details of the elastomer are specified as follows. A slight compressibility is allowed such that its Poisson's ratio is fixed at $\nu_e = 0.49$. To explore the effect of the initial stiffness, E_e, (or, equivalently, the initial shear modulus), five sets of coefficients C_{10}, C_{01}, and D have been used with the corresponding values of E_e/σ_R, E_e, μ_e, and K_e given in Table 1. The values of E_e fall within the range of initial stiffness for polyurea under quasi-static straining (Amirkhizi et al., 2006). Elastomer rate-dependence is not considered. However, as a crude approximation, rate-dependence can be taken into accounted by identifying the modulus with the experimental modulus at strain-rate set by the imposed stretch-rate.

As seen in Table 1, the range of E_e/σ_R in the study is from 0.25 to 1.25. Computations have been made for thickness ratios, $h_e^0/h_m^0 = 1, 2, 3, 4, 5$. Results for the all-metal plate ($h_e^0/h_m^0 = 0$) will also be presented. Calculations have been performed for the following dimensionless stretch rates: $\Lambda = 0.00486$, 0.0243, 0.0486, and 0.0973. For the smallest of these, $\Lambda = 0.00486$, the bilayer behavior is nearly quasi-static, but inertia is important in all the others. It is helpful to interpret the stretch-rates in dimensional terms; for the aluminum layer with $h_m^0 = 0.01$ m, the above dimensionless rates correspond to $\dot{\lambda} = 100\ \text{s}^{-1}$, $500\ \text{s}^{-1}$, $1000\ \text{s}^{-1}$, and $2000\ \text{s}^{-1}$, respectively. In some of the discussion and in the figures which follow, the dimensional stretch-rates will be used (with $h_m^0 = 0.01$ m assumed) together with h_e^0/h_m^0 and E_e/σ_R to identify the parameter set since this combination of parameters is easier to interpret than a set including the dimensionless rate, Λ.

The computational model described above was analyzed using the finite element software ABAQUS Explicit (2004). Large geometry deformations are taken into account in the computational framework. Three-node linear plane strain triangular elements with reduced integration are used for the metal layer and four-node bilinear plane strain elements with reduced integration are used for the elastomer layer. For all cases, nodes are almost uniformly distributed over each layer of the plate with the distance between two neighboring nodes being approximately $h_m^0/20$. As described before, a constant, uniform horizontal velocity V_0 is applied to the right end of the bilayer plate. The initial velocity condition detailed by Xue et al. (in press) is imposed, along with zero displacement at each node at $t = 0$.

3. Neck evolution of the bilayer plate subjected to dynamic stretching

3.1. General features of neck development in the bilayer

To introduce some of the main features of neck development in a bilayer subject to dynamic stretching, we begin by considering a bilayer with $h_e^0/h_m^0 = 3$ and $E_e/\sigma_R = 1$ subject to a high stretch-rate, $\dot{\lambda} = 1000\ \text{s}^{-1}$

($\Lambda = 0.0486$). Fig. 3 illustrates the evolution of distribution of the local logarithmic strain, ε_{11}, of line elements originally at X_1, along and parallel to the mid-line of the metal layer. Very early in the deformation history, the strains are almost uniformly distributed. When the overall logarithmic strain, defined as $\bar{\varepsilon} = \ln \lambda$, increases to 0.2, plastic localization begins at the weakest section of the metal layer, displayed as an elevation of the local strain underneath the initial notch at $X_1 = 0$. As the plate deforms further with $\bar{\varepsilon} = 0.4$, significant necking occurs in the metal layer at the initial location, but a second neck is observed centered a distance about $3.3h_m^0$ away from the mid-point of the first neck, measured in the original configuration. (In the current geometry this distance is about $3.3\lambda h_m^0$ or $4.9h_m^0$.) Between the two largest peaks in the strain, there is a section having minimum local strain marked as B in Fig. 3. During the period when the overall strain increases from 0.4 to 0.6, almost no straining occurs at B, while the strains at the center of the first and second necks undergo significant increase. During this same period, a third neck and even a forth neck form in the metal layer. Finally, as the overall strain increases from $\bar{\varepsilon} = 0.8$ to $\bar{\varepsilon} = 1$, further localization ceases, and everywhere along the plate the local strains increase at almost the same rate as the overall strain rate. Throughout the entire history, the material to the right of the necks, $X_1/h_m^0 > 12$, deforms almost uniformly with $\varepsilon_{11} \cong \bar{\varepsilon}$.

For reference, we note that an all-metal layer of this material with no elastomer layer and stretched quasi-statically would begin to neck when $\bar{\varepsilon} \cong N = 0.02$ (the Considere condition). Moreover, elastic unloading outside the neck would start at the beginning of necking, localization would continue unabated in neck, and the strain outside the neck would never exceed $\bar{\varepsilon} \cong N = 0.02$ (see ahead to Fig. 7). Both the elastomer and inertia contribute to the development of large strains $\varepsilon_{11} \cong \bar{\varepsilon}$ in the dynamically stretched bilayer outside the neck in Fig. 3. Loss of load carrying capacity of the metal within the neck is shed to the elastomer because its incremental stiffness does not diminish with stretch (Xue and Hutchinson, 2007). At sufficiently large strains (i.e., $\bar{\varepsilon} \cong 0.8$ in Fig. 3), the elastomer becomes incrementally stiffer than the metal and from then on the elastomer layer controls the deformation. For its part, inertia slows contraction within the neck, delaying localization and allowing continuing plastic deformation outside the neck (Shenoy and Freund, 1999). It is notable that the computational model predicts the development of multiple, almost equally spaced necks, even though

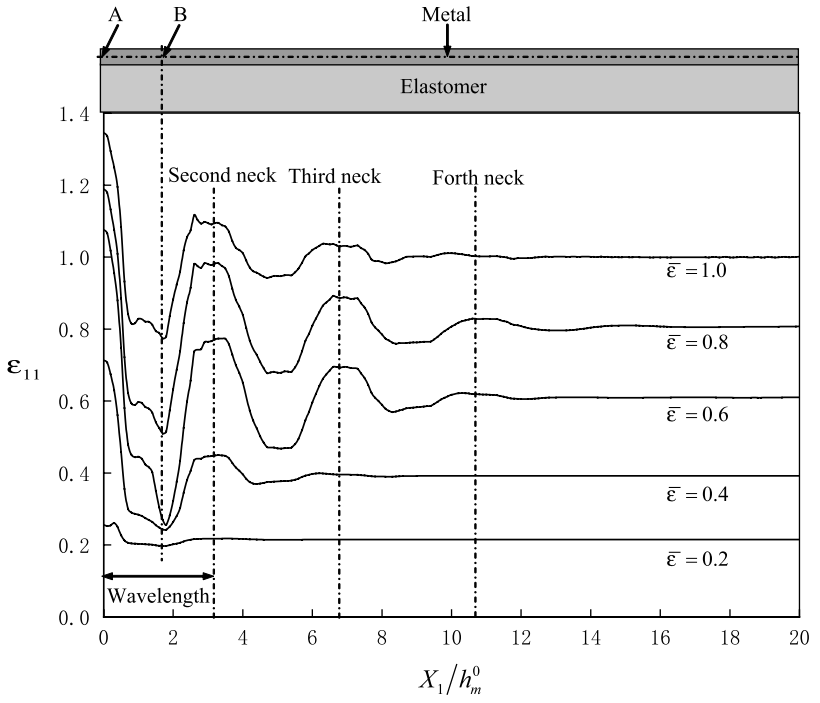

Fig. 3. Distribution of the logarithmic stretching strain in the middle of the metal layer at various overall strains $\bar{\varepsilon}$. The distribution is plotted as a function of the location of the material points in the undeformed configuration, X_1. These results apply to the specific case with $\dot{\lambda} = 1000\ \mathrm{s}^{-1}$, $h_c^0/h_m^0 = 3$, and $E_c/\sigma_R = 1$.

the imperfection is prescribed only at $X_1 = 0$ and has much smaller length than the spacing between necks, i.e., $0.4h_m^0$ vs. $3.3h_m^0$ for the example in Fig. 3. This spacing, measured in the undeformed geometry, is close to the wavelength of very small sinusoidal imperfections that give rise to the largest finite amplitude necks predicted for dynamically stretched monolithic metal plates at similar dimensionless stretch rates, Λ (Xue et al., in press). Moreover, experimental observations of multiple necks in dynamically stretched strips display a similar range of wavelengths (Zhang and Ravi-Chandar, 2006). For the example in Fig. 3, the spacing between necks is controlled by inertia and not the stiffness of the elastomer as will be clear from discussion which follows.

3.2. The combined roles of the elastomer layer and inertia on necking in the bilayer

In this sub-section, the development of necking will be tracked by plotting the strain history in the middle of the metal layer of the main neck at A, ε_{11}^A, against the strain, ε_{11}^B, at the material point B at the middle of the metal layer where the minimum strain occurs (Fig. 3). After the onset of necking the value of ε_{11}^A is always much larger than the overall strain $\bar{\varepsilon}$ while ε_{11}^B is slightly lower than $\bar{\varepsilon}$.

The effect of the thickness ratio h_e^0/h_m^0 on neck evolution in the bilayer plate is investigated first for plates with $E_e/\sigma_R = 1$ and $\dot{\lambda} = 1000\ s^{-1}$ ($\Lambda = 0.0486$). The local stretching strains at points A and B, are presented as a function of overall logarithmic strain $\bar{\varepsilon}$ for various values of h_e^0/h_m^0 in Fig. 4. As reference, the results for the all-metal plate ($h_e^0/h_m^0 = 0$) are also included. For the all-metal plate, little evidence of necking is seen until $\bar{\varepsilon} \cong 0.1$. Straining at B ceases at $\varepsilon_{11}^B \cong 0.16$ when $\bar{\varepsilon} \cong 0.18$, and this serves as an effective definition for the overall strain at necking. Note that this necking strain with $\Lambda = 0.0486$ is much larger than the quasi-static necking strain for the all-metal plate, i.e., $\bar{\varepsilon} \cong N = 0.02$.

For a bilayer plate with equal thicknesses, $h_e^0/h_m^0 = 1$, the onset of necking is at $\bar{\varepsilon} \cong 0.21$ corresponding to a local strain at point B, $\varepsilon_{11}^B \cong 0.18$, both of which are somewhat higher than that for the all-metal plate. Once the elastomer layer is three times the thickness of the metal layer, further increases of the elastomer layer have no further effect on necking retardation – the elastomer is effectively infinitely thick. This is consistent with the finding based on inspection of the numerical results that the distribution of strain in the elastomer layer becomes nearly uniform at depths more than about two metal-layer-thicknesses from the bilayer interface. In addition, contrary to the behavior of the all-metal plate wherein all subsequent straining occurs in the neck until the cross-section goes to zero, straining in the bilayers occurs both inside and outside the neck (i.e., at A and B) after the overall strain reaches sufficiently large values. As discussed earlier, this occurs when the

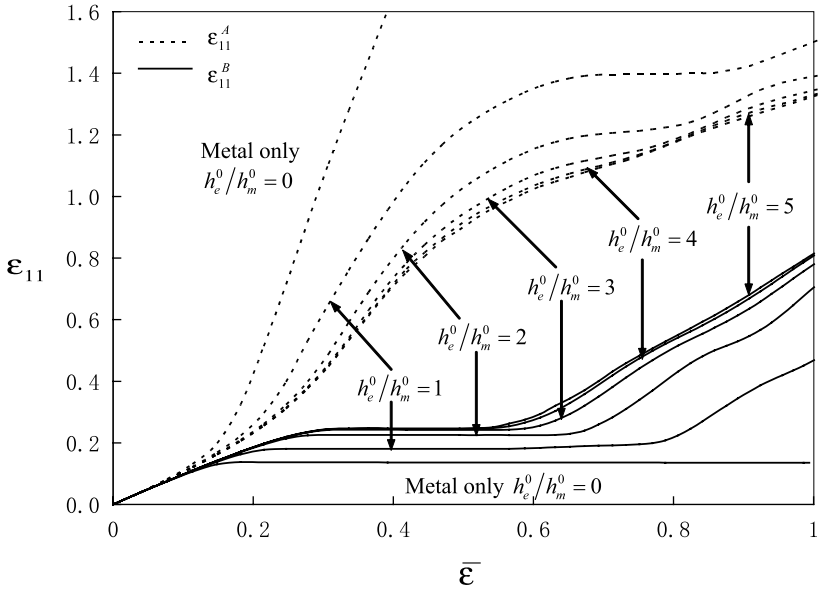

Fig. 4. Stretching strains at sites A and B, ε_{11}^A and ε_{11}^B, as a function of the overall strain $\bar{\varepsilon}$ for $\dot{\lambda} = 1000\ s^{-1}$ and $E_e/\sigma_R = 1$. The six pairs of curves correspond to the six ratios h_e^0/h_m^0, including that for an all-metal plate.

incremental elastomer stiffness dominates behavior, and localization within the metal layer is then significantly mitigated.

The features discussed above are seen in the deformed configurations for three thicknesses of the elastomer layer in Fig. 5 plotted at an overall logarithmic strain of $\bar{\varepsilon} = 0.7$. Here, again, the horizontal locations of the material points have been mapped onto the coordinate X_1 in the underformed state. The lack of dependence of the spacing between the multiple necks on the elastomer thickness at this stretch-rate is evident, as is the near-planarity of the lower surface of the elastomer for the case $h_e^0/h_m^0 = 3$.

The role of the elastomer modulus is seen in Fig. 6 for a bilayer plate with $h_e^0/h_m^0 = 3$ subjected to dynamic stretching with a constant stretch rate $\dot{\lambda} = 1000\ \mathrm{s}^{-1}$ ($\Lambda = 0.0486$). The ratio E_e/σ_R ranges from 0.25 to 1.25. For bilayers having $E_e/\sigma_R \leqslant 0.5$, the deformation outside the neck at B ceases "forever" after the onset of necking, similar to the behavior of the all-metal plate. However, for $E_e/\sigma_R > 0.5$, the elastomer is sufficiently stiff such that the phenomenon noted above occurs wherein the elastomer imposes a nominally uniform incremental stretch-rate on the metal layer at overall strains above some level. For $E_e/\sigma_R = 1.25$, the plate undergoes nearly uniform extension over the entire range of straining. The elastomer is sufficiently thick and stiff such that necking is mitigated entirely.

The role of the overall stretch-rate, $\dot{\lambda}$, is explored in Fig. 7 for bilayers having $E_e/\sigma_R = 1$ and the full range of thickness ratios. As noted previously, the stretch-rates, $\dot{\lambda} = 100\ \mathrm{s}^{-1}$, $500\ \mathrm{s}^{-1}$ and $1000\ \mathrm{s}^{-1}$, for a metal layer with $h_m^0 = 0.01\mathrm{m}$ correspond to dimensionless rates, $\Lambda = 0.00486$, 0.0243 and 0.0486, respectively. Fig. 7 plots the strain, ε_{11}^B, at the location of minimum strain, B, outside the neck. Two values

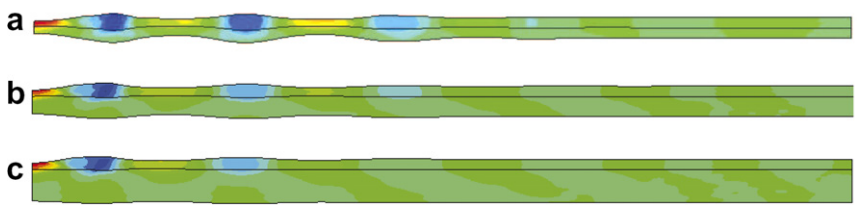

Fig. 5. Deformed configurations for three thicknesses of the elastomer layer at $\bar{\varepsilon} = 0.7$ for $E_e/\sigma_R = 1$ and $\dot{\lambda} = 1000\ \mathrm{s}^{-1}$: (a) $h_e^0/h_m^0 = 1$; (b) $h_e^0/h_m^0 = 2$; (c) $h_e^0/h_m^0 = 3$. Horizontal locations are mapped onto the locations of the material points in the undeformed state.

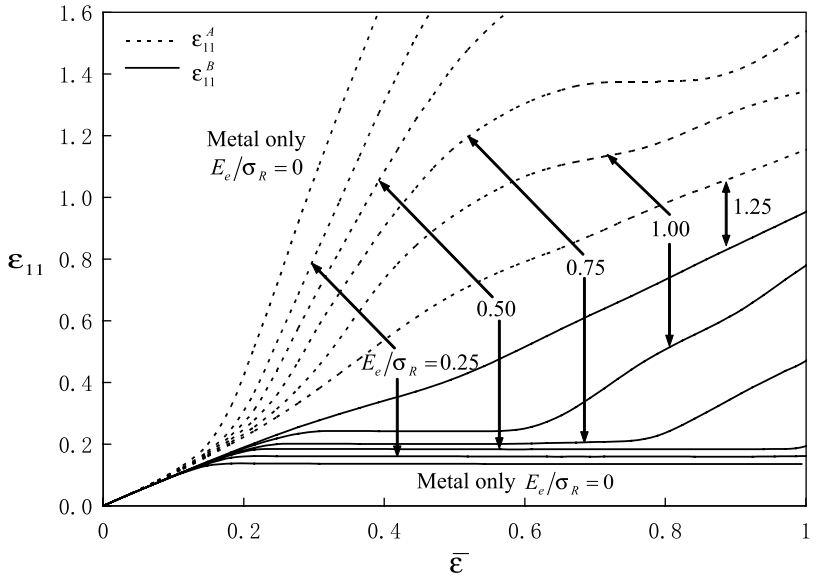

Fig. 6. Stretching strains at sites A and B, ε_{11}^A and ε_{11}^B, as a function of the overall strain $\bar{\varepsilon}$ for $\dot{\lambda} = 1000\ \mathrm{s}^{-1}$ and $h_e^0/h_m^0 = 3$. The six pairs of curves correspond to the six ratios E_e/σ_R, including that for an all-metal plate.

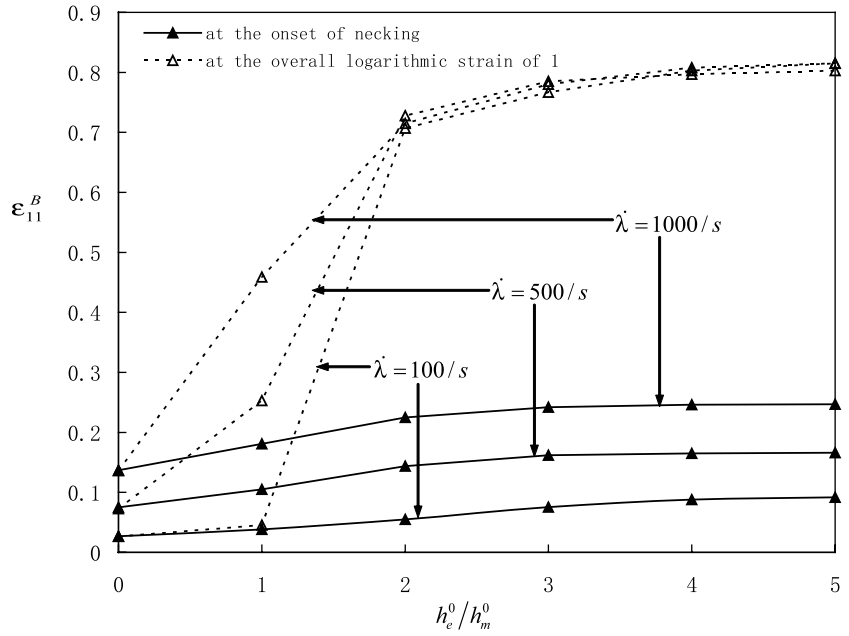

Fig. 7. The influence of elastomer thickness on necking retardation at three stretch rates. The strain, ε_{11}^{B}, in the middle of the metal layer at site B corresponding to the location of minimum strain is plotted at the onset of necking and at an overall strain $\bar{\varepsilon} = 1$. The results for $\dot{\lambda} = 100\ s^{-1}$ are nearly quasi-static. In all cases, $E_e/\sigma_R = 1$.

of ε_{11}^{B} are displayed: (i) that at the onset of necking, i.e., the point at which ε_{11}^{B} first ceases to increase, and (ii) ε_{11}^{B} when the overall strain attains $\bar{\varepsilon} = 1$. As mentioned earlier, inertia has almost no effect on the results for $\dot{\lambda} = 100\ s^{-1}$, and these results are effectively the quasi-static limit. As can be seen in Fig. 7, the overall stain at the onset of necking in an all-metal plate stretched quasi-statically is $\bar{\varepsilon} \cong 0.02$, in accord with the Considere criterion as previously discussed. Moreover, ε_{11}^{B} remains unchanged as the overall strain is increased beyond the onset of necking because all the straining takes place in the neck. Inertia alone ($h_e^0/h_m^0 = 0$) raises the strain at the onset of necking, but it does not enable further straining outside the neck after the onset. Under quasi-static stretching ($\dot{\lambda} = 100\ s^{-1}$ in Fig. 7), the elastomer layer gives rise to a modest increase in the overall strain at the onset of necking and enables further straining to occur outside the neck after the onset of necking if $h_e^0/h_m^0 > 1$. Inertia and an elastomer layer in combination give rise to both a significant delay in the onset of necking and substantial straining outside the neck following the onset of necking.

A similar plot reveals the interaction between stretch-rate and elastomer modulus in Fig. 8 for elastomer layers with $h_e^0/h_m^0 = 3$. At low E_e/σ_R the onset of necking is dominated by inertia and localized straining in the necks does not saturate as overall stretch proceeds. However, at higher E_e/σ_R, the elastomer stiffness causes saturation of localized straining. The higher the stretch-rate, the lower the elastomer stiffness required to produce saturation. At the highest stretch-rate shown, $\dot{\lambda} = 2000\ s^{-1}$ ($\Lambda = 0.097$), saturation effects occur for $E_e/\sigma_R > 0.25$.

Deformed configurations at the overall strain $\bar{\varepsilon} = 0.7$ illustrating the roles of stretch-rate and elastomer stiffness are shown in Fig. 9, in all cases with $h_e^0/h_m^0 = 3$. Fig. 9a and b for nominally quasi-static stretching ($\dot{\lambda} = 100\ s^{-1}$) reveal that the spacing between necks is controlled by the elastomer stiffness as analyzed in detail by Li and Suo, 2006. The stiffer elastomer reduces the amplitudes of the necks. At $\bar{\varepsilon} = 0.7$, necks have formed along the entire length of the bilayer. In the absence of the elastomer layer, a single neck would form at the imperfection. Fig. 9c and d for a high rate of stretch ($\dot{\lambda} = 1000\ s^{-1}$) show that the elastomer stiffness influences the amplitudes of the necks and the intensity of non-uniform deformation in the elastomer, but not the spacing between the necks. As noted earlier, at high rates of stretch the inertia of the metal layer appears to control the neck spacing.

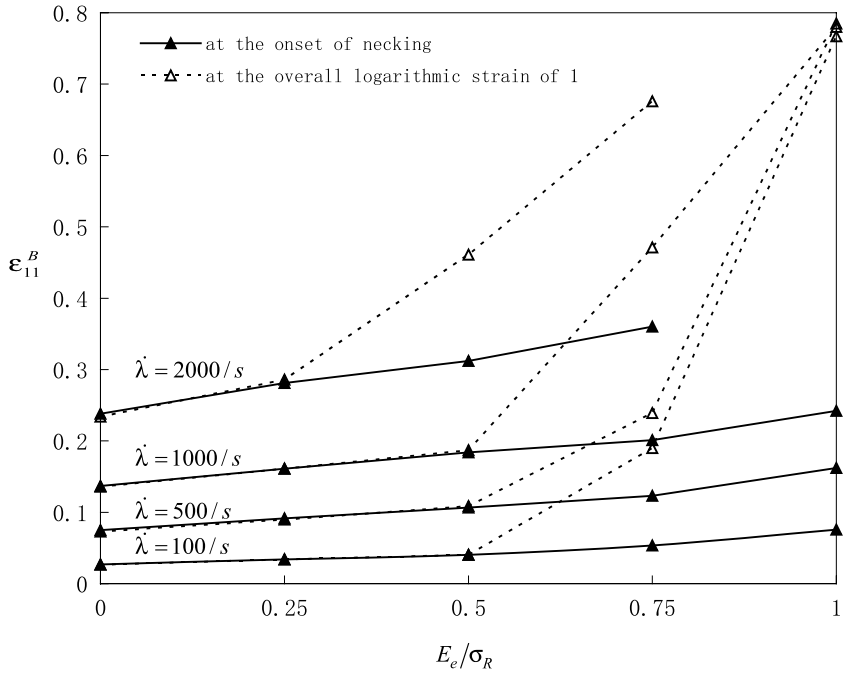

Fig. 8. The influence of elastomer stiffness on necking retardation at four overall stretch rates. The stretching strain at site B is plotted at the onset of necking and at the overall strain $\bar{\varepsilon} = 1$. The thickness ratio h_e^0/h_m^0 is fixed at 3. The limit $E_e/\sigma_R = 0$ applies to the all-metal plate, and the results for $\dot{\lambda} = 100\ s^{-1}$ are nearly quasi-static.

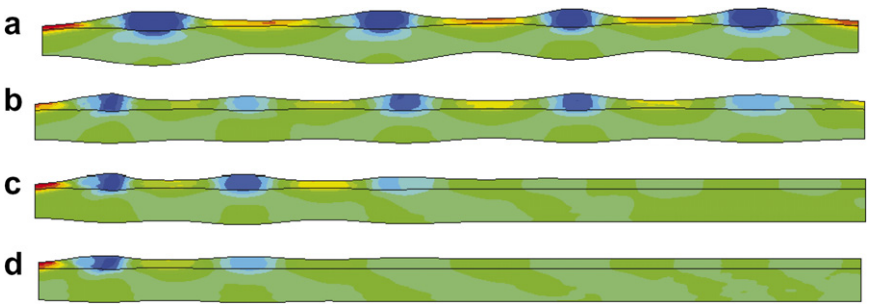

Fig. 9. Deformed configurations at $\bar{\varepsilon} = 0.7$. Horizontal locations have been mapped to the location of material points in the undeformed state. All bilayers have $h_e^0/h_m^0 = 3$. (a) $\dot{\lambda} = 100\ s^{-1}$ and $E_e/\sigma_R = 0.75$; (b) $\dot{\lambda} = 100\ s^{-1}$ and $E_e/\sigma_R = 1$; (c) $\dot{\lambda} = 1000\ s^{-1}$ and $E_e/\sigma_R = 0.75$; (d) $\dot{\lambda} = 1000\ s^{-1}$ and $E_e/\sigma_R = 1$. The configurations for $\dot{\lambda} = 100\ s^{-1}$ are essentially identical to those expected under quasi-static stretching.

4. Conclusions

The elastomer layer and the inertia associated with dynamic stretching both contribute to neck retardation in the metal layer and both give rise to multiple necks. In addition, a sufficiently stiff elastomer layer is capable of limiting the localized strain in the necks in the metal layer after the onset of necking. The interaction between the elastomer layer and inertia is not simple, in part because there are several parameters specifying the system. In all the examples presented here, the density ratio has been fixed at $\rho_e/\rho_m = 0.407$, representative of an elastomer/aluminum bilayer. The important remaining dimensionless parameters, Λ, E_e/σ_R, and h_e^0/h_m^0, have been identified in (4). A brief summary of their influences follows.

(i) For quasi-static stretching ($\Lambda << 0.01$), the extent of retardation of the onset of necking is approximately proportional to $h_e^0 E_e / h_m^0 \sigma_R$ (Xue and Hutchinson, 2007; Li and Suo, 2006). A rough requirement on the elastomer layer such that it limits localization of strain within the necks in the metal layer is $h_e^0 E_e / h_m^0 \sigma_R > 1$, as can be inferred from the results presented.

(ii) In the absence of the elastomer layer, inertia gives rise to neck retardation and to the formation of multiple necks if $\Lambda > 0.01$ (Shenoy and Freund, 1999; Xue et al., in press).

(iii) For dynamic stretching of the bilayer, inertia appears to be the dominant factor controlling retardation of the onset of necking and the spacing between the necks when $\Lambda > 0.01$. Limitation of localized straining within the necks by the elastomer requires (approximately) $h_e^0 E_e / h_m^0 \sigma_R > 1$.

The above conclusions are predicated on the assumption that the elastomer is adequately represented by the Mooney–Rivlin or Neo-Hookean constitutive relation within the range of strains which necking occurs. Specifically, it is essential that the incremental stiffness of the elastomer in the relevant range of strains correlates with the ground state modulus, E_e, in the manner inferred from these constitutive models. If the elastomer has less incremental stiffness than implied by the models its effectiveness in retarding the onset of necking and in limiting localization will be reduced. Recent experimental data of Roland et al. (2007) for a polyurea that has been considered for limiting localization and fracture in bilayers suggests that this material undergoes yield-like behavior at strains on the order of 0.1 and does not maintain the incremental stiffness implied by the Mooney–Rivlin or Neo-Hookean relations. If acceptable elastomers (or polymers) can be identified for this purpose, one notes that for bilayers having equal thicknesses of metal and elastomer, the controlling parameter is the ratio of elastomer modulus to metal flow stress at a strain of unity, E_e/σ_R. The higher the strength the metal, the more difficult it will be to identify an elastomer or polymer that can retard necking.

Acknowledgements

This work was supported in part by ONR Grant N00014-04-1-0154 and in part by the School of Engineering and Applied Sciences, Harvard University. Z.X. acknowledges support from Department of Engineering Mechanics, Tsinghua University, China.

References

ABAQUS, 2004. ABAQUS/Explicit User's Manual Version 6.5, ABAQUS Inc.

Amirkhizi, Z.V., Isaacs, J., McGee, J., Nemat-Nasser, S., 2006. An experimentally-based viscoelastic constitutive model for polyurea, including pressure and temperature effects. Philos. Mag. 86, 5847–5866.

Hutchinson, J.W., Neale, K.W., 1977. Influence of strain-rate sensitivity on necking under uniaxial tension. Acta Metall. 25, 839–846.

Li, T., Suo, Z., 2006. Deformability of thin metal films on elastomer substrates. Int. J. Solids Struct. 43, 2351–2363.

Needleman, A., 1991. The effect of material inertia on neck development. In: Yang, W.H. (Ed.), Topics in Plasticity. AM Press, Ann Arbor, MI, pp. 151–160.

Roland, C.M., Twigg, J.N., Vu, Y., Mott, P.H., 2007. High strain rate mechanical behavior of polyurea. Polymer 48, 574.

Shenoy, V.B., Freund, L.B., 1999. Necking bifurcations during high strain rate extension. J. Mech. Phys. Solids 47, 2209–2233.

Woodford, D.A., 1969. Strain-rate sensitivity as a measure of ductility (Strain-rate sensitivity measurements to determine ductility of materials, noting relation to elongation.). ASM. Trans. Quar. 62, 291–293.

Xue, Z., Hutchinson, Z.W., 2007. Neck retardation and enhanced energy absorption in metal–elastomer bilayers. Mech. Mater. 39, 473–487.

Xue, Z., Vaziri, A., Hutchinson, J.W., in press. Material aspects of dynamic neck retardation. J. Mech. Phys. Solids.

Zhang, H., Ravi-Chandar, K., 2006. On the dynamic of necking and fragmentation – I. Real-time and post-mortem observations in Al 6061-O. Int. J. Fracture 142, 183–217.